

M³: A Modular World Model over Streams of Tokens

Lior Cohen¹ Kaixin Wang^{*2} Bingyi Kang³ Uri Gadot¹ Shie Mannor^{*1}

Abstract

Token-based world models emerged as a promising modular framework, modeling dynamics over token streams while optimizing tokenization separately. While successful in visual environments with discrete actions (e.g., Atari games), their broader applicability remains uncertain. In this paper, we introduce M³, a **modular world model** that extends this framework, enabling flexible combinations of observation and action modalities through independent modality-specific components. M³ integrates several improvements from existing literature to enhance agent performance. Through extensive empirical evaluation across diverse benchmarks, M³ achieves state-of-the-art sample efficiency for planning-free world models. Notably, among these methods, it is the first to reach a human-level median score on Atari 100K, with superhuman performance on 13 games. We [open-source our code and weights](#).

1. Introduction

Modeling the dynamics of the world has been a long-standing and compelling topic in reinforcement learning, with foundational ideas proposed over 30 years ago (Sutton, 1991; Schmidhuber, 1991; 2010). It has been leveraged to enhance planning performance (Schrittwieser et al., 2019), produce fictitious data for policy training (Hafner et al., 2023), or simulate interactive experiences (DeepMind, 2024; Decart et al., 2024; Agarwal et al., 2025).

In this study, we focus on *token-based* world models (TBWMs) (Micheli et al., 2023; 2024; Cohen et al., 2024), sample-efficient reinforcement learning (RL) methods that learn the dynamics entirely within a learned token space. TBWMs offer a clear modularity between the representation and the dynamics by separating their optimization. Such modularity provides a clean and efficient way to unify different observation modalities within a shared token space,

^{*}Equal advising ¹Technion – Israel Institute of Technology ²Microsoft Research ³ByteDance Seed. Correspondence to: Lior Cohen <liorcohen5@campus.technion.ac.il>.

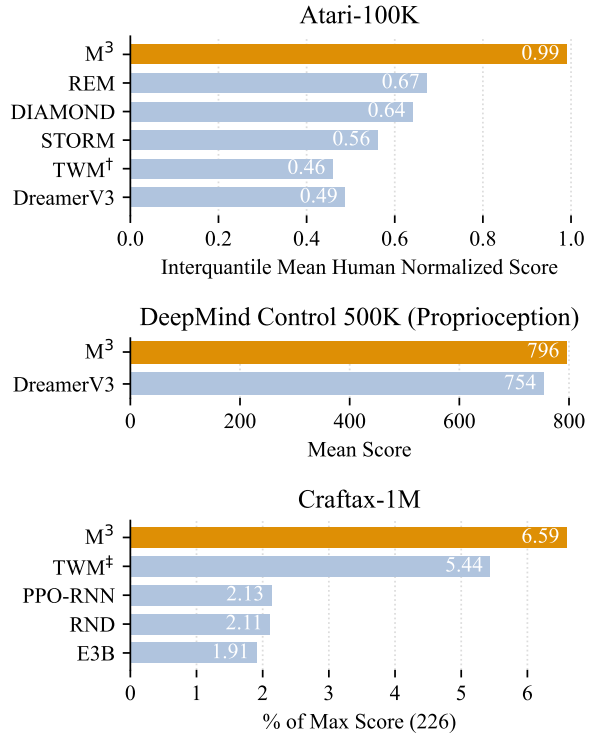


Figure 1: Results overview. M³ exhibits state-of-the-art sample-efficiency performance for planning-free methods across all three benchmarks. † (Robine et al., 2023), ‡ (Dedieu et al., 2025).

offloading representation learning to the tokenizer design step. More generally, modular systems are easier to scale, develop, evaluate, and deploy, as individual modules can be treated independently and are easier to master through divide and conquer.

While TBWMs hold promise as a general framework for handling different modalities, existing work primarily focuses on image observations and discrete actions, such as Atari games. It remains unclear whether token-based world models are truly effective for handling diverse modalities and how to design the model to achieve it. This limits the broader adoption of token-based models.

To address these limitations, we propose a **modular world model**, termed M³, which implements a modular framework

for general-purpose token-based world models. Specifically, M^3 maintains a set of independent modality-specific tokenizers, embedding tables, and prediction heads to handle various modalities. This modular design allows M^3 to process any combination of observation and action modalities.

In addition, M^3 combines several recent improvements from the literature. Specifically, the control policy is intrinsically motivated to reduce the epistemic uncertainty of the world model (Shyam et al., 2019; Sekar et al., 2020), a world model replay buffer further improves sample efficiency (Kauvar et al., 2023), and continuous values are predicted via classification models (Farebrother et al., 2024; Hafner et al., 2023).

To validate the effectiveness of our method, we conducted extensive empirical evaluations across three diverse benchmarks, ranging from the visual Atari 100K, to the continuous proprioception tasks of the DeepMind Control Suite, to Craftax, which combines symbolic 2D grid maps with continuous state features. There, M^3 achieves state-of-the-art sample-efficiency for planning-free world models. Ablation studies further show the contribution of each component.

Summary of contributions:

- We propose M^3 , a widely applicable token-based world model agent that follows a modular framework.
- We conduct extensive empirical evaluation, providing strong evidence for the effectiveness of TBWMs as general methods. There, M^3 achieves state-of-the-art (planning-free) performance across all benchmarks.
- To facilitate future research and broader adoption of TBWMs, we open-source our code and trained models.

2. Method

Notations We consider the Partially Observable Markov Decision Process (POMDP) setting. However, since in practice the agent has no knowledge about the hidden state space, consider the following state-agnostic formulation. Let Ω, \mathcal{A} be the sets of observations and actions, respectively. At every step t , the agent observes $\mathbf{o}_t \in \Omega$ and picks an action $\mathbf{a}_t \in \mathcal{A}$. From the agent’s perspective, the environment evolves according to $\mathbf{o}_{t+1}, r_t, d_t \sim p(\mathbf{o}_{t+1}, r_t, d_t | \mathbf{o}_{\leq t}, \mathbf{a}_{\leq t})$, where r_t, d_t are the observed reward and termination signals, respectively. The process repeats until a positive termination signal $d_t \in \{0, 1\}$ is obtained. The agent’s objective is to maximize its expected return $\mathbb{E}[\sum_{t=0}^{\infty} \gamma^t r_{t+1}]$ where $\gamma \in [0, 1]$ is a discount factor.

For multi-modal observations, let $\mathbf{o}_t = \{\mathbf{o}_t^{(i)}\}_{i=1}^{|\kappa|}$ where κ is the set of environment modalities and $\mathbf{o}_t^{(i)}$ denotes the features of modality κ_i .

Overview M^3 builds on REM (Cohen et al., 2024). The agent comprises a representation module \mathcal{V} , a world model \mathcal{M} , a controller \mathcal{C} , and a replay buffer. To facilitate a modular design, following REM, each module is optimized separately. The training process of the agent involves a repeated cycle of four steps: data collection, representation learning (\mathcal{V}), world model learning (\mathcal{M}), and control learning in imagination (\mathcal{C}).

2.1. The Representation Module \mathcal{V}

\mathcal{V} is responsible for encoding and decoding raw observations and actions. It is a modular tokenization system with encoder-decoder pairs for different input modalities. Encoders produce fixed-length token sequences, creating a common interface that enables combining tokens from various sources into a unified representation. After embedding, these token sequences are concatenated into a single representation, as described in Section 2.2. Note that encoder-decoder pairs need not be learning-based methods. Although learned pairs are optimized independently. This design enables \mathcal{V} to deal with any combination of input modalities, provided the respective encoder-decoder pairs.

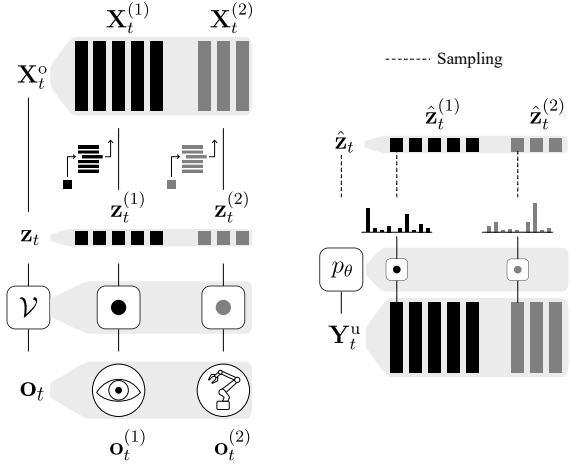
Tokenization \mathcal{V} transforms raw observations \mathbf{o} to sets of fixed-length integer token sequences $\mathbf{z} = \{\mathbf{z}^{(i)}\}_{i=1}^{|\kappa|}$ by applying the encoder of each modality $\mathbf{z}^{(i)} = \text{enc}_i(\mathbf{o}^{(i)})$. Actions \mathbf{a} are tokenized using the encoder-decoder pair of the related modality to produce \mathbf{z}^a . The respective decoders reconstruct observations from their tokens: $\hat{\mathbf{o}}^{(i)} = \text{dec}_i(\mathbf{z}^{(i)})$.

M^3 natively supports four modalities: images, continuous vectors, categorical variables, and image-like multi-channel grids of categorical variables, referred to as "2D categoricals". More formally, 2D categoricals are elements of $([k_1] \times [k_2] \times \dots \times [k_C])^{m \times n}$ where k_1, \dots, k_C are per channel vocabulary sizes, C is the number of channels, m, n are spatial dimensions, and $[k] = \{1, \dots, k\}$.

Following REM, we use a VQ-VAE (Esser et al., 2021; van den Oord et al., 2017) for image observations. For the tokenization of continuous vectors, each feature is quantized to produce a token, as in (Reed et al., 2022). Unbounded vectors are first transformed using the symlog function (Hafner et al., 2023), defined as $\text{symlog}(x) = \text{sign}(x) \ln(1 + |x|)$, which compresses the magnitude of large absolute values. Lastly, while no special tokenization is required for categorical inputs, 2D categoricals are flattened along the spatial dimensions to form a sequence of categorical vectors. The embedding of each token vector is obtained by averaging the embeddings of its entries.

2.2. The World Model \mathcal{M}

The purpose of \mathcal{M} is to learn a model of the environment’s dynamics. Concretely, given trajectory segments



(a) Tokenization and embedding. (b) Observation prediction.

Figure 2: An illustration of the independent processing of modalities for an observation with two modalities.

$\tau_t = \mathbf{z}_1, \mathbf{z}_1^a, \dots, \mathbf{z}_t, \mathbf{z}_t^a$ in token representation, \mathcal{M} models the distributions of the next observation and termination signal, and the expected reward:

$$\text{Transition: } p_\theta(\hat{\mathbf{z}}_{t+1} | \tau_t), \quad (1)$$

$$\text{Reward: } \hat{r}_t = \hat{r}_\theta(\tau_t), \quad (2)$$

$$\text{Termination: } p_\theta(\hat{d}_t | \tau_t). \quad (3)$$

where θ is the parameters vector of \mathcal{M} and $\hat{r}_\theta(\tau_t)$ is an estimator of $\mathbb{E}_{r_t \sim p(r_t | \tau_t)}[r_t]$.

Architecture \mathcal{M} comprises a sequence model f_θ and multiple heads for the prediction of tokens of different observation modalities, rewards, termination signals, and for the estimation of model uncertainty. Concretely, f_θ is a retentive network (RetNet) (Sun et al., 2023) augmented with a parallel observation prediction (POP) (Cohen et al., 2024) mechanism. All heads are implemented as multilayer perceptrons (MLP) with a single hidden layer. We defer the details about these architectures to Appendix A.3.

Embedding \mathcal{M} translates token trajectories τ into sequences of d -dimensional embeddings \mathbf{X} using a set of embedding (look-up) tables. By design, each modality is associated with a separate table. In cases where an embedding table is not provided by the appropriate encoder-decoder pair, \mathcal{M} and \mathcal{C} learn dedicated tables separately and independently. As embeddings sequences are composed hierarchically, we use the following hierarchical notation:

$$\text{Observation-action block: } \mathbf{X}_t = (\mathbf{X}_t^o, \mathbf{X}_t^a)$$

$$\text{Observation block: } \mathbf{X}_t^o = (\mathbf{X}_t^{(1)}, \dots, \mathbf{X}_t^{(|\kappa|)})$$

where K_i denotes the number of embedding vectors in $\mathbf{X}_t^{(i)}$. Similarly, $K = \sum_{i=1}^{|\kappa|} K_i$. To combine latents of each \mathbf{z}_t , \mathcal{V} concatenates their token sequences along the temporal axis based on a predefined modality order. We defer the full details on the embedding process to Appendix A.3.

Sequence Modeling Given a sequence of observation-action blocks $\mathbf{X} = \mathbf{X}_1, \dots, \mathbf{X}_t$, the matching outputs $\mathbf{Y}_1, \dots, \mathbf{Y}_t$ are computed auto-regressively as follows:

$$(\mathbf{S}_t, \mathbf{Y}_t) = f_\theta(\mathbf{S}_{t-1}, \mathbf{X}_t)$$

where \mathbf{S}_t is a recurrent state that summarizes $\mathbf{X}_{\leq t}$ and $\mathbf{S}_0 = 0$. However, the output \mathbf{Y}_{t+1}^u , from which $\hat{\mathbf{z}}_{t+1}$ is predicted, is computed using the POP mechanism via another call as

$$(\cdot, \mathbf{Y}_{t+1}^u) = f_\theta(\mathbf{S}_t, \mathbf{X}^u)$$

where $\mathbf{X}^u \in \mathbb{R}^{K \times d}$ is a learned embedding sequence. Intuitively, \mathbf{X}^u acts as a learned prior, enabling the parallel generation of multiple tokens into the future.

To model $p_\theta(\hat{\mathbf{z}}_{t+1} | \mathbf{Y}_{t+1}^u)$, the distributions $p_\theta(\hat{z} | \mathbf{y})$ of each token \hat{z} of $\hat{\mathbf{z}}_{t+1}^{(i)}$ of each modality κ_i are modeled using modality-specific prediction heads implemented as MLPs with a single hidden layer and an output size equal to the vocabulary size of enc_i (Figure 2b). For 2D categoricals, C heads are used to predict the C tokens from each \mathbf{y} .

Similarly, rewards and termination signals are predicted by additional prediction heads as $\hat{r}_t = \hat{r}_\theta(\mathbf{y})$, $\hat{d}_t \sim p_\theta(\hat{d}_t | \mathbf{y})$, slightly abusing notations, where \mathbf{y} is the last vector of \mathbf{Y}_{t+1}^u . An illustration is provided in Figure 3.

Reducing Epistemic Uncertainty via Intrinsic Motivation The world model \mathcal{M} serves as the cornerstone of the entire system. Any controller operating within a world model framework can only perform as well as the underlying world model allows, making its quality a fundamental limiting factor. In deep learning methods, the model’s performance depends heavily on the quality of its training data. Accurate dynamics modeling requires comprehensive data collection that captures the full spectrum of possible environmental behaviors. This presents a particular challenge in online RL, where the controller must systematically and efficiently explore its environment. Success depends on intelligently guiding the controller toward unexplored or undersampled regions of the dynamics space. An effective approach to this challenge involves estimating the world model’s epistemic uncertainty and directing the controller to gather data from regions where this uncertainty is highest (Schmidhuber, 2010; Shyam et al., 2019; Sekar et al., 2020).

Our approach estimates epistemic uncertainty using an ensemble of $N_{\text{ens}} = 4$ next observation prediction heads $\{p_{\phi_i}(\hat{\mathbf{z}} | \text{sg}(\mathbf{Y}^u))\}_{i=1}^{N_{\text{ens}}}$ with parameters $\{\phi_i\}_{i=1}^{N_{\text{ens}}}$ (Sekar et al.,

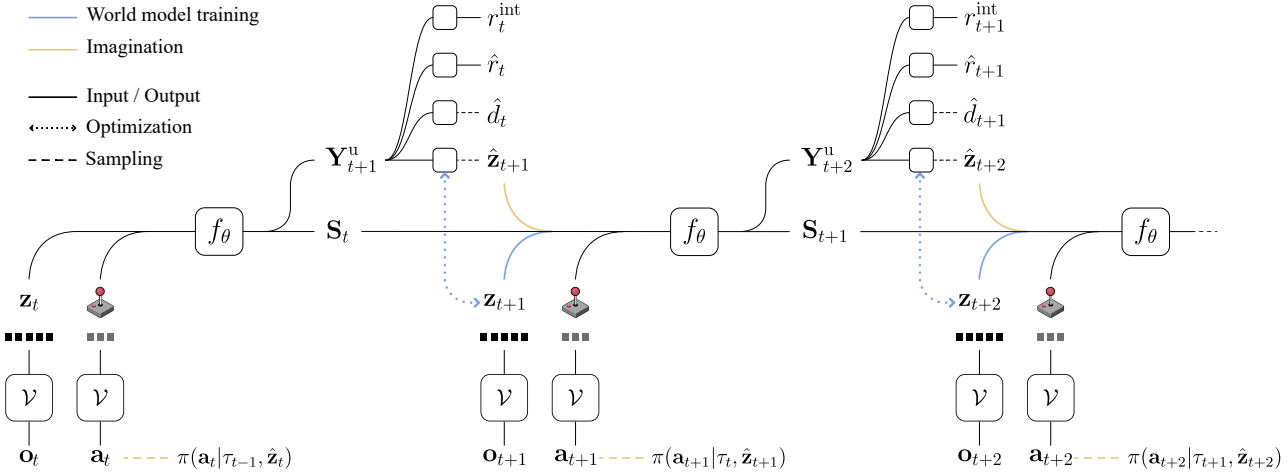


Figure 3: World model training and imagination. To maintain visual clarity, we omitted token embedding details, as well as optimization details of rewards and termination signals.

2020; Lakshminarayanan et al., 2017) where $\text{sg}(\cdot)$ is the stop gradient operator. To quantify disagreement between the ensemble’s distributions, we employ the Jensen-Shannon divergence (JSD) (Shyam et al., 2019). For probability distributions P_1, \dots, P_n , the JSD is defined as:

$$\text{JSD}(P_1, \dots, P_n) = \mathcal{H}\left(\frac{1}{n} \sum_{i=1}^n P_i\right) - \frac{1}{n} \sum_{i=1}^n \mathcal{H}(P_i)$$

where $\mathcal{H}(\cdot)$ denotes the Shannon entropy. Since observations comprise multiple tokens, we average the per-token JSD values to obtain a single uncertainty measure δ_t . Training data is divided equally among ensemble members, with each predictor processing a distinct subset of each batch. Despite the ensemble approach, our implementation maintains computational efficiency, with negligible additional overhead in practice.

To guide \mathcal{C} towards regions of high epistemic uncertainty, \mathcal{M} provides \mathcal{C} with additional intrinsic rewards $r_t^{\text{int}} = \delta_t$ during imagination. Here, the reward provided by \mathcal{M} at each step t is given by

$$\bar{r}_t = w^{\text{int}} r_t^{\text{int}} + w^{\text{ext}} \hat{r}_t$$

where $w^{\text{int}}, w^{\text{ext}} \in \mathbb{R}$ are hyperparameters that control the scale of each reward type. Optimizing the controller in imagination allows it to reach areas of high model uncertainty without additional real-environment interaction.

Prioritized Replay Recent work has demonstrated that prioritizing replay buffer sampling during world model training could lead to significant performance gains in intrinsically motivated agents (Kauvar et al., 2023). While their approach showed promise, it required extensive hyperparameter tuning in practice. We propose a simpler, more robust prioritization scheme for world model training.

Here, the replay buffer maintains a world model loss value for each stored example, with newly added examples assigned a high initial loss value of 10. During \mathcal{M} ’s training, we sample each batch using a mixture of uniform and prioritized sampling, controlled by a single parameter $\alpha \in [0, 1]$ that determines the fraction of prioritized samples. For the prioritized portion, we sample examples proportional to their softmax-transformed losses $p_i = \text{softmax}(\mathcal{L})_i$. The loss values are updated after each world model optimization step using the examples’ current batch losses.

Training We use the cross-entropy loss for the optimization of all components of \mathcal{M} . Specifically, for each t , the loss of $p_\theta(\hat{\mathbf{z}}_t | \mathbf{Y}_t^u)$ is obtained by averaging the cross-entropy losses of its individual tokens. The same loss is used for each ensemble member $p_{\phi_i}(\hat{\mathbf{z}}_t | \text{sg}(\mathbf{Y}_t^u))$. The optimization and design of the reward predictor is similar to that of the critic, as described in Section 2.3. A formal description of the optimization objective can be found in Appendix A.3.1.

2.3. The Controller \mathcal{C}

\mathcal{C} is an extended version of the actor-critic of REM (Cohen et al., 2024) that supports additional observation and action spaces and integrates a classification-based value prediction.

Architecture At the core of \mathcal{C} ’s architecture, parameterized by ψ , is an LSTM (Hochreiter & Schmidhuber, 1997) sequence model. At each step t , upon observing \mathbf{z}_t , a set of modality-specific encoders map each modality tokens $\mathbf{z}_t^{(i)}$ to a latent vector $\mathbf{x}^{(i)}$, where we abuse our notation \mathbf{x} as the context of the discussion is limited to \mathcal{C} . The latents are then fused by a fully-connected network to obtain a single vector $\mathbf{x} = g_\psi(\mathbf{x}^{(1)}, \dots, \mathbf{x}^{(|\kappa|)})$. $\mathbf{x}_t \in \mathbb{R}^{d_c}$ is processed by \mathcal{C} ’s sequence model to produce

$\mathbf{h}_t, \mathbf{c}_t = \text{LSTM}(\mathbf{x}_t, \mathbf{h}_{t-1}, \mathbf{c}_{t-1}; \psi)$ where $\mathbf{h}_t, \mathbf{c}_t$ are the LSTM’s hidden and cell states, respectively. Lastly, two linear output layers produce the logits from which the actor and critic outputs $\pi(\mathbf{a}_t|\mathbf{h}_t), \hat{V}^\pi(\mathbf{h}_t)$ are derived. For continuous action spaces, the actor uses a categorical distribution over a uniformly spaced discrete subset of $[-1, 1]$. We defer the full details about the encoding process to Appendix A.4.

Classification Based Prediction of Continuous Values

Robustly handling unbounded reward signals has long been challenging as they can vary dramatically in both magnitude and frequency. (Hafner et al., 2023) addressed this challenge by using a classification network that predicts the weights of exponentially spaced bins and employed a two-hot loss for the network’s optimization. (Farebrother et al., 2024) studied the use of cross-entropy loss in place of the traditional mean squared error loss for value-based deep RL methods. In their work, the HL-Gauss method was shown to significantly outperform the two-hot loss method. Following these developments, we adopt (Hafner et al., 2023)’s approach of using a classification network with exponential bins, while implementing the HL-Gauss method for the optimization of the network. Concretely, the critic’s value estimates are predicted using a linear output layer parameterized by $\mathbf{W} \in \mathbb{R}^{m \times d_c}$ with $m = 128$ outputs corresponding to m uniform bins defined by $m + 1$ endpoints $\mathbf{b} = (b_0, \dots, b_m)$. The predicted value is given by

$$\hat{y} = \text{symexp}\left(\text{softmax}(\mathbf{W}\mathbf{h})^\top \hat{\mathbf{b}}\right)$$

where $\text{symexp}(x) = \text{sign}(x)(\exp(|x|) - 1)$ is the inverse of the symlog function and $\hat{\mathbf{b}} = \left(\frac{b_1+b_0}{2}, \dots, \frac{b_m+b_{m-1}}{2}\right)$ are the bin centers. Given the true target $y \in \mathbb{R}$, the HL-Gauss loss is given by

$$\mathcal{L}_{\text{HL-Gauss}}(\mathbf{W}, \mathbf{h}, y) = \tilde{y}^\top \log \text{softmax}(\mathbf{W}\mathbf{h})$$

where $\tilde{y}_i = \Phi\left(\frac{b_i - \text{symlog}(y)}{\sigma}\right) - \Phi\left(\frac{b_{i-1} - \text{symlog}(y)}{\sigma}\right)$, Φ is the cumulative density function of the standard normal distribution and σ is a standard deviation hyperparameter that controls the amount of label smoothing.

Training in Imagination \mathcal{C} is trained entirely from simulated experience generated through interaction with \mathcal{M} . Specifically, \mathcal{M} and \mathcal{C} are initialized with a short trajectory segment sampled uniformly from the replay buffer and interact for H steps. An illustration of this process is given in Figure 3 (orange path). λ -returns are computed for each generated trajectory segment and are used as targets for critic learning. For policy learning, a REINFORCE (Sutton et al., 1999) objective is used, with a \hat{V}^π baseline for variance reduction. See Appendix A.4.2 for further details.

3. Experiments

To evaluate sample efficiency, we used benchmarks that measure performance within a fixed, limited environment interaction budget. The selected benchmarks also addressed two key research questions: (1) whether M^3 performs effectively in continuous environments and (2) whether it handles multi-modal observations successfully.

3.1. Experimental Setup

Benchmarks: We evaluate M^3 on three sample-efficiency benchmarks of different observation and action modalities: Atari 100K (Kaiser et al., 2020), DeepMind Control Suite (DMC) Proprioception 500K (Tunyasuvunakool et al., 2020), and Craftax-1M (Matthews et al., 2024).

Atari 100K has become the gold standard in the literature for evaluating sample-efficient deep RL agents. The benchmark comprises a subset of 26 games. Within each game, agents must learn from visual image signal under a tightly restricted budget of 100K interactions, corresponding to roughly two hours of human gameplay.

The DeepMind Control Suite (DMC) is a set of continuous control tasks involving multiple agent embodiments ranging from simple single-joint models to complex humanoids. Here, we follow the subset of proprioception tasks used for the evaluation of DreamerV3 (Hafner et al., 2023), where observations and actions are continuous vectors. At each task, the agent’s interaction budget is limited to 500K steps.

Craftax is a 2D open-world survival game benchmark inspired by Minecraft, designed to evaluate RL agents’ capabilities in planning, memory, and exploration. The partially-observable environment features procedurally generated worlds where agents must gather and craft resources while surviving against hostile creatures. Observations consist of a 9×11 tile egocentric map, where each tile consists of 4 symbols, and 48 state features corresponding to state information such as inventory and health. Here, we consider the sample-efficiency oriented Craftax-1M variant which only allows an interaction budget of one million steps.

Baselines On Atari-100K, we compare M^3 against DreamerV3 (Hafner et al., 2023) and several methods restricted to image observations: TWM (Robine et al., 2023), STORM (Zhang et al., 2024), DIAMOND (Alonso et al., 2024), and REM (Cohen et al., 2024). On DMC, we compare exclusively with DreamerV3, currently the only planning-free world model method with published results on the 500K proprioception benchmark. On Craftax-1M, we compare against TWM (Dedieu et al., 2025), a concurrent work that proposes a Transformer based world model with a focus on the Craftax benchmark, and the baselines reported in the Craftax paper: Random Network Distillation (RND)

Table 1: Mean returns on the 26 games of the Atari 100k benchmark followed by averaged human-normalized performance metrics. Each game score is computed as the average of 5 runs with different seeds. Bold face mark the best score.

Game	Random	Human	DreamerV3	TWM	STORM	DIAMOND	REM	M ³ (ours)
Alien	227.8	7127.7	959.4	674.6	983.6	744.1	607.2	687.2
Amidar	5.8	1719.5	139.1	121.8	204.8	225.8	95.3	102.4
Assault	222.4	742.0	705.6	682.6	801.0	1526.4	1764.2	1822.8
Asterix	210.0	8503.3	932.5	1116.6	1028.0	3698.5	1637.5	1369.1
BankHeist	14.2	753.1	648.7	466.7	641.2	19.7	19.2	347.1
BattleZone	2360.0	37187.5	12250.0	5068.0	13540.0	4702.0	11826.0	13262.0
Boxing	0.1	12.1	78.0	77.5	79.7	86.9	87.5	93.5
Breakout	1.7	30.5	31.1	20.0	15.9	132.5	90.7	148.9
ChopperCommand	811.0	7387.8	410.0	1697.4	1888.0	1369.8	2561.2	3611.6
CrazyClimber	10780.5	35829.4	97190.0	71820.4	66776.0	99167.8	76547.6	93433.2
DemonAttack	152.1	1971.0	303.3	350.2	164.6	288.1	5738.6	4787.6
Freeway	0.0	29.6	0.0	24.3	0.0	33.3	32.3	31.9
Frostbite	65.2	4334.7	909.4	1475.6	1316.0	274.1	240.5	258.4
Gopher	257.6	2412.5	3730.0	1674.8	8239.6	5897.9	5452.4	4363.2
Hero	1027.0	30826.4	11160.5	7254.0	11044.3	5621.8	6484.8	7466.8
Jamesbond	29.0	302.8	444.6	362.4	509.0	427.4	391.2	678.0
Kangaroo	52.0	3035.0	4098.3	1240.0	4208.0	5382.2	467.6	6656.0
Krull	1598.0	2665.5	7781.5	6349.2	8412.6	8610.1	4017.7	6677.3
KungFuMaster	258.5	22736.3	21420.0	24554.6	26182.0	18713.6	25172.2	31705.4
MsPacman	307.3	6951.6	1326.9	1588.4	2673.5	1958.2	962.5	1282.7
Pong	-20.7	14.6	18.4	18.8	11.3	20.4	18.0	19.9
PrivateEye	24.9	69571.3	881.6	86.6	7781.0	114.3	99.6	100.0
Qbert	163.9	13455.0	3405.1	3330.8	4522.5	4499.3	743.0	2425.6
RoadRunner	11.5	7845.0	15565.0	9109.0	17564.0	20673.2	14060.2	24471.8
Seaquest	68.4	42054.7	618.0	774.4	525.2	551.2	1036.7	1800.4
UpNDown	533.4	11693.2	7567.1	15981.7	7985.0	3856.3	3757.6	10416.5
#Superhuman (↑)	0	N/A	9	8	9	11	12	13
Mean (↑)	0.000	1.000	1.124	0.956	1.222	1.459	1.222	1.645
Median (↑)	0.000	1.000	0.485	0.505	0.425	0.373	0.280	0.982
IQM (↑)	0.000	1.000	0.487	0.459	0.561	0.641	0.673	0.990
Optimality Gap (↓)	1.000	0.000	0.510	0.513	0.472	0.480	0.482	0.412

(Burda et al., 2019), PPO (Schulman et al., 2017) with a recurrent neural network (PPO-RNN), and Exploration via Elliptical Episodic Bonuses (E3B) (Hennaf et al., 2022). As Craftax is a recent benchmark, there are no other published results in existing world models literature. Following the standard practice in the literature, we exclude planning-based methods (Hansen et al., 2024; Wang et al., 2024), as planning is an orthogonal component that operates on any given model, typically incurring significant computational overhead. Here, our focus is on the world model component.

Metrics and Evaluation For Atari, we report human-normalized scores (HNS) $\frac{\text{agent_score} - \text{random_score}}{\text{human_score} - \text{random_score}}$ (Mnih et al., 2015). Following the protocol of (Agarwal et al., 2021) and using their toolkit, we report the mean, median, interquartile mean (IQM), and optimality gap metrics with 95% stratified bootstrap confidence intervals. For DMC and Craftax, we report the raw agent returns. We use 5 random seeds per environment. In each experiment, final performance is evaluated using 100 test episodes at the end of training and the mean score is reported.

3.2. Results

M³ achieves state-of-the-art performance across all three benchmarks (Figure 1). On Atari 100k, M³ outperforms all baselines across all key metrics (Figure 4). Notably, M³ is the first planning-free world model to reach a human-level IQM and median scores. In addition, it achieves superhuman performance on **13** out of 26 games, surpassing all baselines. These results highlight M³'s effectiveness in sample-efficient learning and its robustness across diverse tasks in the Atari 100k benchmark.

Is M³ effective in continuous environments? Figure 4 provides compelling evidence that token-based architectures can indeed excel in continuous domains: M³ achieves performance comparable to DreamerV3 across most tasks, and notably outperforms it on Cartpole Swingup Sparse and both Hopper tasks.

Is M³ effective in environments with multi-modal observations? Since modularity is at the core of M³, we

Title Suppressed Due to Excessive Size

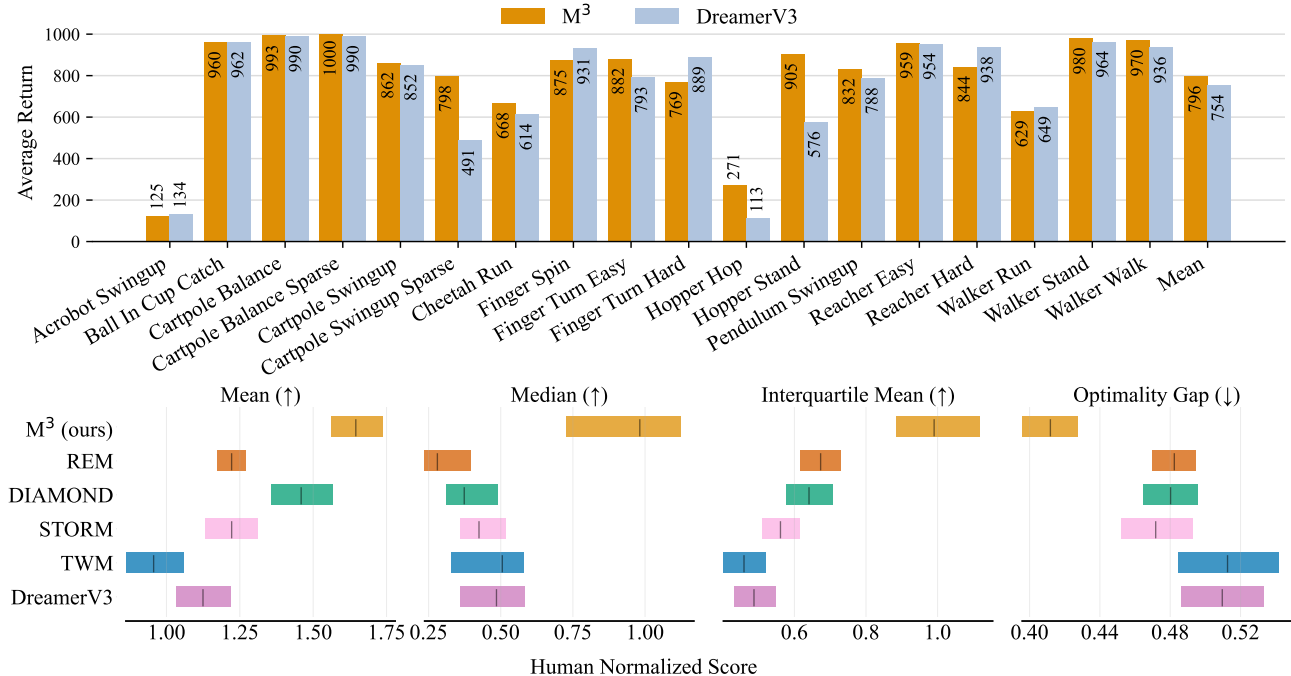


Figure 4: Results on the DeepMind Control Suite 500K Proprioception (top) and Atari 100K (bottom) benchmarks.

investigate its performance in Craftax, as it combines an image-like 2D grid map with a vector of features, involving multiple tokenizers (\mathcal{V}). Figure 5 shows that M^3 maintains sample-efficiency in this multi-modal environment as well, as it significantly outperforms all model-free baselines, including exploration-oriented ones. M^3 also attains state-of-the-art performance even compared to concurrent world model methods (Figure 1). With 444 tokens per observation arranged into 147 sequences, even short trajectories in Craftax contain thousands of tokens, demonstrating M^3 's efficient handling of long sequences.

3.3. Ablation Studies

We ablate the intrinsic rewards, prioritized replay, and classification-based predictions to demonstrate their individual contributions to M^3 's performance. In each ablation, M^3 is modified so that only the component of interest is disabled. Due to limited computational resources, we consider a subset of 8 tasks for each of the Atari 100K and DMC benchmarks. Concretely, for Atari 100K, we used "Assault", "Breakout", "Chopper Command", "Crazy Climber", "James bond", "Kangaroo", "Seaquest", and "Up'n Down", in which significant improvements were observed. For DMC, we chose a subset that includes different embodiments: "acrobot swingup", "cartpole swingup sparse", "cheetah run", "finger turn hard", "hopper stand", "pendulum swingup", "reacher hard", and "walker run".

The results are presented in Figure 6. Although all components contributed to the final performance of M^3 , the intrinsic rewards proved crucial for achieving competitive performance, particularly on DMC.

More broadly, the results in Figure 6 demonstrate that encouraging the controller to explore regions of high epistemic uncertainty through intrinsic rewards significantly improves its performance in world model agents, even in reward-rich environments. This observation is non-trivial in a sample-efficiency setting, as model-driven exploration costs the agent some amount of interaction budget, which could be otherwise used for controller-driven exploration during data collection. The latter type of exploration aims to collect new information about the true reward signal, which defines the task and its success metric. On the other hand, model-driven exploration may guide the controller towards environment regions that are irrelevant to the task at hand.

4. Related Work

Offline Multi-Modal Methods Large-scale token-based sequence models for modeling and generating multi-modal trajectories of agent experience were proposed in (Lu et al., 2023; 2024; Reed et al., 2022; Schubert et al., 2023). In Gato (Reed et al., 2022) and TDM (Schubert et al., 2023), multi-modal inputs are first tokenized through predefined transformations, while in Unified IO (Lu et al., 2023; 2024) pretrained models are also used. The produced tokens are

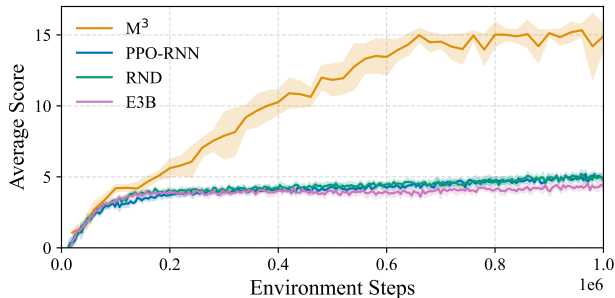


Figure 5: Craftax-1M training curves with mean and 95% confidence intervals.

then embedded and processed by the sequence model, similarly to M^3 . Importantly, these methods do not learn control through RL. Instead, they learn from expert data. In addition, these methods use large models with billions of parameters, large vocabulary sizes, and orders-of-magnitude more data and compute compared to sample efficient world models. Hence, it is unclear whether the design choices of these methods would be effective in an online sample-efficiency setting, where the data is non-stationary and strictly limited.

World Model Agents Model-based RL agents where the policy is learned exclusively from simulated data generated by the learned world model were originally proposed by (Ha & Schmidhuber, 2018). Later, a line of works proposed the popular Dreamer algorithms (Hafner et al., 2020; 2021; 2023). To learn dynamics, Dreamer’s objective involves a Kullback–Leibler (KL) divergence term between its learned prior and posterior estimators, effectively coupling the optimization of the representation model and the recurrent neural network world model. This design leads to a complex monolithic system that poses challenges for development and scaling.

Following the success of the Transformer architecture (Vaswani et al., 2017) in language modeling (Brown et al., 2020), Transformer-based variants of Dreamer (Zhang et al., 2024; Robine et al., 2023) were proposed. In addition, token-based world models (TBWMs), which represent trajectories as language-like token sequences, were proposed (Micheli et al., 2023; Cohen et al., 2024). Notably, the evaluation of these methods is limited to the Atari 100K benchmark.

Recently, motivated by the success of diffusion generative models (Rombach et al., 2022), DIAMOND (Alonso et al., 2024), a diffusion-based world model agent was proposed. Although it produces visually compelling outputs, it is currently limited to visual environments.

Large Video World Models Following recent advances in video generative modeling (Ho et al., 2022; Blattmann et al., 2023; Brooks et al., 2024), a recent body of work proposed

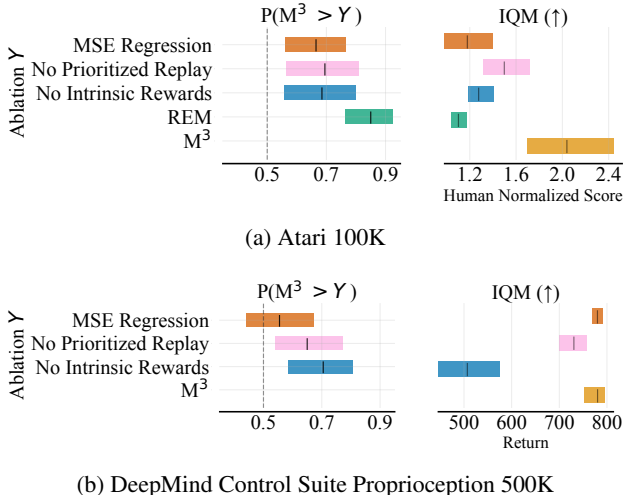


Figure 6: Ablations results on the Atari-100K (top) and DeepMind Control Proprioception 500K (bottom) benchmarks. A subset of 8 games was used for each ablation.

large video world models (DeepMind, 2024; Agarwal et al., 2025; Decart et al., 2024; Valevski et al., 2024). These methods are trained offline on massive pre-collected data to predict future video frames. However, these methods do not involve control learning, and RL in particular.

5. Limitations and Future Work

Here, we briefly highlight several limitations of this work. First, since rich multi-modal RL benchmarks are scarce, future work could wrap multiple single-modality environments into a unified multi-modal environment, which can be used to evaluate agents under different modality combinations as well as the agent’s ability to perform multiple independent tasks concurrently.

Second, although the feature quantization approach for tokenizing continuous vectors showed promise, it leads to excessive sequence lengths. We believe that more efficient solutions can be found for dealing with continuous inputs.

6. Conclusions

In this paper, we proposed a modular world model, M^3 , for sample-efficient RL. M^3 extends token-based world model agents via a modular framework to support a wide range of environments and modalities. In addition, it combines multiple advances from existing literature to enhance performance. Through extensive empirical evaluation, M^3 exhibited state-of-the-art performance for planning-free world models on a diverse set of benchmarks, involving visual, continuous, and structured symbolic modalities. Notably, on the well-established Atari-100K benchmark, M^3 outper-

formed all baselines across all metrics.

7. Impact Statement

This paper presents work whose goal is to advance the field of Machine Learning. There are many potential societal consequences of our work, none which we feel must be specifically highlighted here.

References

- Agarwal, N., Ali, A., Bala, M., Balaji, Y., Barker, E., Cai, T., Chattopadhyay, P., Chen, Y., Cui, Y., Ding, Y., et al. Cosmos world foundation model platform for physical ai. *arXiv preprint arXiv:2501.03575*, 2025.
- Agarwal, R., Schwarzer, M., Castro, P. S., Courville, A. C., and Bellemare, M. Deep reinforcement learning at the edge of the statistical precipice. In Ranzato, M., Beygelzimer, A., Dauphin, Y., Liang, P., and Vaughan, J. W. (eds.), *Advances in Neural Information Processing Systems*, volume 34, pp. 29304–29320. Curran Associates, Inc., 2021. URL https://proceedings.neurips.cc/paper_files/paper/2021/file/f514cec81cb148559cf475e7426eed5e-Paper.pdf.
- Alonso, E., Jelley, A., Micheli, V., Kanervisto, A., Storkey, A., Pearce, T., and Fleuret, F. Diffusion for world modeling: Visual details matter in atari. *arXiv preprint arXiv:2405.12399*, 2024.
- Bengio, Y., Léonard, N., and Courville, A. Estimating or propagating gradients through stochastic neurons for conditional computation. *arXiv preprint arXiv:1308.3432*, 2013.
- Blattmann, A., Dockhorn, T., Kulal, S., Mendelevitch, D., Kilian, M., Lorenz, D., Levi, Y., English, Z., Voleti, V., Letts, A., et al. Stable video diffusion: Scaling latent video diffusion models to large datasets. *arXiv preprint arXiv:2311.15127*, 2023.
- Brooks, T., Peebles, B., Holmes, C., DePue, W., Guo, Y., Jing, L., Schnurr, D., Taylor, J., Luhman, T., Luhman, E., Ng, C., Wang, R., and Ramesh, A. Video generation models as world simulators. 2024. URL <https://openai.com/research/video-generation-models-as-world-simulators>.
- Brown, T., Mann, B., Ryder, N., Subbiah, M., Kaplan, J. D., Dhariwal, P., Neelakantan, A., Shyam, P., Sastry, G., Askell, A., Agarwal, S., Herbert-Voss, A., Krueger, G., Henighan, T., Child, R., Ramesh, A., Ziegler, D., Wu, J., Winter, C., Hesse, C., Chen, M., Sigler, E., Litwin, M., Gray, S., Chess, B., Clark, J., Berner, C., McCandlish, S., Radford, A., Sutskever, I., and Amodei, D. Language models are few-shot learners. In Larochelle, H., Ranzato, M., Hadsell, R., Balcan, M., and Lin, H. (eds.), *Advances in Neural Information Processing Systems*, volume 33, pp. 1877–1901. Curran Associates, Inc., 2020. URL https://proceedings.neurips.cc/paper_files/paper/2020/file/1457c0d6bfc4967418bfb8ac142f64a-Paper.pdf.
- Burda, Y., Edwards, H., Storkey, A., and Klimov, O. Exploration by random network distillation. In *International Conference on Learning Representations*, 2019. URL <https://openreview.net/forum?id=H1lJJnR5Ym>.
- Cohen, L., Wang, K., Kang, B., and Mannor, S. Improving token-based world models with parallel observation prediction. In *Forty-first International Conference on Machine Learning*, 2024. URL <https://openreview.net/forum?id=Lfp5Dk1xb6>.
- Decart, Quevedo, J., McIntyre, Q., Campbell, S., Chen, X., and Wachen, R. Oasis: A universe in a transformer, 2024. URL <https://oasis-model.github.io/>.
- Dedieu, A., Ortiz, J., Lou, X., Wendelken, C., Lehrach, W., Guntupalli, J. S., Lazaro-Gredilla, M., and Murphy, K. P. Improving transformer world models for data-efficient rl, 2025. URL <https://arxiv.org/abs/2502.01591>.
- DeepMind, G. Genie 2: A large-scale foundation world model, 2024. URL <https://deepmind.google/discover/blog/genie-2-a-large-scale-foundation-world-model/>.
- Esser, P., Rombach, R., and Ommer, B. Taming transformers for high-resolution image synthesis. In *Proceedings of the IEEE/CVF conference on computer vision and pattern recognition*, pp. 12873–12883, 2021.
- Farebrother, J., Orbay, J., Vuong, Q., Taiga, A. A., Chebotar, Y., Xiao, T., Irpan, A., Levine, S., Castro, P. S., Faust, A., Kumar, A., and Agarwal, R. Stop regressing: Training value functions via classification for scalable deep RL. In *Forty-first International Conference on Machine Learning*, 2024. URL <https://openreview.net/forum?id=dVpFKfqF3R>.
- Ha, D. and Schmidhuber, J. Recurrent world models facilitate policy evolution. In *Advances in Neural Information Processing Systems 31*, pp. 2451–2463. Curran Associates, Inc., 2018. URL <https://papers.nips.cc/paper/7512-recurrent-world-models-facilitate-policy-evolution>. <https://worldmodels.github.io>.

- Hafner, D., Lillicrap, T., Ba, J., and Norouzi, M. Dream to control: Learning behaviors by latent imagination. In *International Conference on Learning Representations*, 2020. URL <https://openreview.net/forum?id=S1l0TC4tDS>.
- Hafner, D., Lillicrap, T. P., Norouzi, M., and Ba, J. Mastering atari with discrete world models. In *9th International Conference on Learning Representations, ICLR 2021, Virtual Event, Austria, May 3-7, 2021*. OpenReview.net, 2021. URL <https://openreview.net/forum?id=0oabwyZbOu>.
- Hafner, D., Pasukonis, J., Ba, J., and Lillicrap, T. Mastering diverse domains through world models. *arXiv preprint arXiv:2301.04104*, 2023.
- Hansen, N., Su, H., and Wang, X. TD-MPC2: Scalable, robust world models for continuous control. In *The Twelfth International Conference on Learning Representations*, 2024. URL <https://openreview.net/forum?id=0xh5CstDJU>.
- Henaff, M., Raileanu, R., Jiang, M., and Rocktäschel, T. Exploration via elliptical episodic bonuses. In Oh, A. H., Agarwal, A., Belgrave, D., and Cho, K. (eds.), *Advances in Neural Information Processing Systems*, 2022. URL <https://openreview.net/forum?id=Xg-yZos9qJQ>.
- Hendrycks, D. and Gimpel, K. Bridging nonlinearities and stochastic regularizers with gaussian error linear units, 2017. URL <https://openreview.net/forum?id=Bk0MRI5lg>.
- Ho, J., Chan, W., Saharia, C., Whang, J., Gao, R., Gritsenko, A., Kingma, D. P., Poole, B., Norouzi, M., Fleet, D. J., et al. Imagen video: High definition video generation with diffusion models. *arXiv preprint arXiv:2210.02303*, 2022.
- Hochreiter, S. and Schmidhuber, J. Long short-term memory. *Neural computation*, 9(8):1735–1780, 1997.
- Johnson, J., Alahi, A., and Fei-Fei, L. Perceptual losses for real-time style transfer and super-resolution. In *Computer Vision—ECCV 2016: 14th European Conference, Amsterdam, The Netherlands, October 11-14, 2016, Proceedings, Part II 14*, pp. 694–711. Springer, 2016.
- Kaiser, Ł., Babaeizadeh, M., Miłoś, P., Osiniński, B., Campbell, R. H., Czechowski, K., Erhan, D., Finn, C., Koza-kowski, P., Levine, S., Mohiuddin, A., Sepassi, R., Tucker, G., and Michalewski, H. Model based reinforcement learning for atari. In *International Conference on Learning Representations*, 2020. URL <https://openreview.net/forum?id=S1xCPJHtDB>.
- Katharopoulos, A., Vyas, A., Pappas, N., and Fleuret, F. Transformers are RNNs: Fast autoregressive transformers with linear attention. In III, H. D. and Singh, A. (eds.), *Proceedings of the 37th International Conference on Machine Learning*, volume 119 of *Proceedings of Machine Learning Research*, pp. 5156–5165. PMLR, 13–18 Jul 2020. URL <https://proceedings.mlr.press/v119/katharopoulos20a.html>.
- Kauvar, I., Doyle, C., Zhou, L., and Haber, N. Curious replay for model-based adaptation. In *Proceedings of the 40th International Conference on Machine Learning, ICML’23*. JMLR.org, 2023.
- Lakshminarayanan, B., Pritzel, A., and Blundell, C. Simple and scalable predictive uncertainty estimation using deep ensembles. In Guyon, I., Luxburg, U. V., Bengio, S., Wallach, H., Fergus, R., Vishwanathan, S., and Garnett, R. (eds.), *Advances in Neural Information Processing Systems*, volume 30. Curran Associates, Inc., 2017. URL https://proceedings.neurips.cc/paper_files/paper/2017/file/9ef2ed4b7fd2c810847ffa5fa85bce38-Paper.pdf.
- Larsen, A. B. L., Sønderby, S. K., Larochelle, H., and Winther, O. Autoencoding beyond pixels using a learned similarity metric. In Balcan, M. F. and Weinberger, K. Q. (eds.), *Proceedings of The 33rd International Conference on Machine Learning*, volume 48 of *Proceedings of Machine Learning Research*, pp. 1558–1566. New York, New York, USA, 20–22 Jun 2016. PMLR. URL <https://proceedings.mlr.press/v48/larsen16.html>.
- Lu, J., Clark, C., Zellers, R., Mottaghi, R., and Kembhavi, A. UNIFIED-IO: A unified model for vision, language, and multi-modal tasks. In *The Eleventh International Conference on Learning Representations*, 2023. URL <https://openreview.net/forum?id=E01k9048soZ>.
- Lu, J., Clark, C., Lee, S., Zhang, Z., Khosla, S., Marten, R., Hoiem, D., and Kembhavi, A. Unified-io 2: Scaling autoregressive multimodal models with vision language audio and action. In *Proceedings of the IEEE/CVF Conference on Computer Vision and Pattern Recognition (CVPR)*, pp. 26439–26455, June 2024.
- Matthews, M., Beukman, M., Ellis, B., Samvelyan, M., Jackson, M., Coward, S., and Foerster, J. Craftax: A lightning-fast benchmark for open-ended reinforcement learning. In *International Conference on Machine Learning (ICML)*, 2024.
- Micheli, V., Alonso, E., and Fleuret, F. Transformers are sample-efficient world models. In *The Eleventh International Conference on Learning Representations*,

- ICLR 2023, Kigali, Rwanda, May 1-5, 2023*. OpenReview.net, 2023. URL <https://openreview.net/pdf?id=vhFulAcb0xb>.
- Micheli, V., Alonso, E., and Fleuret, F. Efficient world models with context-aware tokenization. In *Forty-first International Conference on Machine Learning, ICML 2024, Vienna, Austria, July 21-27, 2024*. OpenReview.net, 2024. URL <https://openreview.net/forum?id=BiWIERWBFX>.
- Mnih, V., Kavukcuoglu, K., Silver, D., Rusu, A. A., Veness, J., Bellemare, M. G., Graves, A., Riedmiller, M., Fidjeland, A. K., Ostrovski, G., et al. Human-level control through deep reinforcement learning. *nature*, 518(7540): 529–533, 2015.
- Paszke, A., Gross, S., Massa, F., Lerer, A., Bradbury, J., Chanan, G., Killeen, T., Lin, Z., Gimelshein, N., Antiga, L., Desmaison, A., Köpf, A., Yang, E., DeVito, Z., Raison, M., Tejani, A., Chilamkurthy, S., Steiner, B., Fang, L., Bai, J., and Chintala, S. Pytorch: An imperative style, high-performance deep learning library. In *Advances in Neural Information Processing Systems*, volume 32, 2019.
- Ramachandran, P., Zoph, B., and Le, Q. V. Searching for activation functions, 2018. URL <https://openreview.net/forum?id=SkBYyZRZ>.
- Reed, S., Zolna, K., Parisotto, E., Colmenarejo, S. G., Novikov, A., Barth-maroon, G., Giménez, M., Sulsky, Y., Kay, J., Springenberg, J. T., Eccles, T., Bruce, J., Razavi, A., Edwards, A., Heess, N., Chen, Y., Hadsell, R., Vinyals, O., Bordbar, M., and de Freitas, N. A generalist agent. *Transactions on Machine Learning Research*, 2022. ISSN 2835-8856. URL <https://openreview.net/forum?id=likK0kHjvj>. Featured Certification, Outstanding Certification.
- Robine, J., Höftmann, M., Uelwer, T., and Harmeling, S. Transformer-based world models are happy with 100k interactions. *arXiv preprint arXiv:2303.07109*, 2023.
- Rombach, R., Blattmann, A., Lorenz, D., Esser, P., and Ommer, B. High-resolution image synthesis with latent diffusion models. In *Proceedings of the IEEE/CVF Conference on Computer Vision and Pattern Recognition (CVPR)*, pp. 10684–10695, June 2022.
- Schmidhuber, J. Curious model-building control systems. In *[Proceedings] 1991 IEEE International Joint Conference on Neural Networks*, pp. 1458–1463 vol.2, 1991. doi: 10.1109/IJCNN.1991.170605.
- Schmidhuber, J. Formal theory of creativity, fun, and intrinsic motivation (1990-2010). *IEEE Transactions on Autonomous Mental Development*, 2, 2010. ISSN 19430604. doi: 10.1109/TAMD.2010.2056368.
- Schrittwieser, J., Antonoglou, I., Hubert, T., Simonyan, K., Sifre, L., Schmitt, S., Guez, A., Lockhart, E., Hassabis, D., Graepel, T., Lillicrap, T., and Silver, D. Mastering atari, go, chess and shogi by planning with a learned model. *NATURE*, 2019. doi: 10.1038/s41586-020-03051-4.
- Schubert, I., Zhang, J., Bruce, J., Bechtle, S., Parisotto, E., Riedmiller, M., Springenberg, J. T., Byravan, A., Hasenclever, L., and Heess, N. A generalist dynamics model for control. *arXiv preprint arXiv:2305.10912*, 2023.
- Schulman, J., Wolski, F., Dhariwal, P., Radford, A., and Klimov, O. Proximal policy optimization algorithms. *arXiv preprint arXiv:1707.06347*, 2017.
- Sekar, R., Rybkin, O., Daniilidis, K., Abbeel, P., Hafner, D., and Pathak, D. Planning to explore via self-supervised world models. In III, H. D. and Singh, A. (eds.), *Proceedings of the 37th International Conference on Machine Learning Research*, volume 119 of *Proceedings of Machine Learning Research*, pp. 8583–8592. PMLR, 13–18 Jul 2020. URL <https://proceedings.mlr.press/v119/sekar20a.html>.
- Shyam, P., Jaśkowski, W., and Gomez, F. Model-based active exploration. In Chaudhuri, K. and Salakhutdinov, R. (eds.), *Proceedings of the 36th International Conference on Machine Learning*, volume 97 of *Proceedings of Machine Learning Research*, pp. 5779–5788. PMLR, 09–15 Jun 2019. URL <https://proceedings.mlr.press/v97/shyam19a.html>.
- Sun, Y., Dong, L., Huang, S., Ma, S., Xia, Y., Xue, J., Wang, J., and Wei, F. Retentive network: A successor to transformer for large language models. *arXiv preprint arXiv:2307.08621*, 2023.
- Sutton, R. S. Dyna, an integrated architecture for learning, planning, and reacting. *ACM SIGART Bulletin*, 2, 1991. ISSN 0163-5719. doi: 10.1145/122344.122377.
- Sutton, R. S., McAllester, D., Singh, S., and Mansour, Y. Policy gradient methods for reinforcement learning with function approximation. In Solla, S., Leen, T., and Müller, K. (eds.), *Advances in Neural Information Processing Systems*, volume 12. MIT Press, 1999. URL https://proceedings.neurips.cc/paper_files/paper/1999/file/464d828b85b0bed98e80ade0a5c43b0f-Paper.pdf.

Tunyasuvunakool, S., Muldal, A., Doron, Y., Liu, S., Bohez, S., Merel, J., Erez, T., Lillicrap, T., Heess, N., and Tassa, Y. dm_control: Software and tasks for continuous control. *Software Impacts*, 6:100022, 2020. ISSN 2665-9638. doi: <https://doi.org/10.1016/j.simpa.2020.100022>. URL <https://www.sciencedirect.com/science/article/pii/S2665963820300099>.

Valevski, D., Leviathan, Y., Arar, M., and Fruchter, S. Diffusion models are real-time game engines. *CoRR*, abs/2408.14837, 2024. URL <https://doi.org/10.48550/arXiv.2408.14837>.

van den Oord, A., Vinyals, O., and kavukcuoglu, k. Neural discrete representation learning. In Guyon, I., Luxburg, U. V., Bengio, S., Wallach, H., Fergus, R., Vishwanathan, S., and Garnett, R. (eds.), *Advances in Neural Information Processing Systems*, volume 30. Curran Associates, Inc., 2017. URL https://proceedings.neurips.cc/paper_files/paper/2017/file/7a98af17e63a0ac09ce2e96d03992fbc-Paper.pdf.

Vaswani, A., Shazeer, N., Parmar, N., Uszkoreit, J., Jones, L., Gomez, A. N., Kaiser, L. u., and Polosukhin, I. Attention is all you need. In Guyon, I., Luxburg, U. V., Bengio, S., Wallach, H., Fergus, R., Vishwanathan, S., and Garnett, R. (eds.), *Advances in Neural Information Processing Systems*, volume 30. Curran Associates, Inc., 2017. URL https://proceedings.neurips.cc/paper_files/paper/2017/file/3f5ee243547dee91fbd053c1c4a845aa-Paper.pdf.

Wang, S., Liu, S., Ye, W., You, J., and Gao, Y. Efficientzero v2: Mastering discrete and continuous control with limited data. In *Forty-first International Conference on Machine Learning*, 2024. URL <https://openreview.net/forum?id=LHGMXcr6zx>.

Zhang, W., Wang, G., Sun, J., Yuan, Y., and Huang, G. Storm: Efficient stochastic transformer based world models for reinforcement learning. *Advances in Neural Information Processing Systems*, 36, 2024.

A. Models and Hyperparameters

A.1. Hyperparameters

We detail shared hyperparameters in Table 2, training hyperparameters in Table 3, world model hyperparameters in Table 4, and controller hyperparameters in Table 5. Environment hyperparameters are detailed in Table 6 (Atari-100K) and Table 7 (DMC).

Tuning Due to limited computational resources, M^3 was not properly tuned. We believe that proper tuning could further improve M^3 's performance.

Table 2: Shared hyperparameters.

Description	Symbol	Value
Eval sampling temperature		0.5
Optimizer		AdamW
Learning rate ($\mathcal{V}, \mathcal{M}, \mathcal{C}$)		(1e-4, 2e-4, 2e-4)
AdamW β_1		0.9
AdamW β_2		0.999
Gradient clipping threshold ($\mathcal{V}, \mathcal{M}, \mathcal{C}$)		(10, 3, 3)
Weight decay ($\mathcal{V}, \mathcal{M}, \mathcal{C}$)		(0.01, 0.05, 0.01)
Prioritized replay fraction	α	0.3
\mathcal{M} ensemble size	N_{ens}	4
HL-Gauss num bins		128
Label smoothing	σ	$\frac{3}{4} \text{bin_width} = 0.1758$

Table 3: Training hyperparameters.

Description	Symbol	Atari-100K	DMC	Craftax
Horizon	H	10	20	20
Observation sequence length	K	64	3-24	147
Action sequence length	K_a	1	1-6	1
Tokenizer vocabulary size	N	512	125	(37,5,40,20,4,125)
Epochs		600	1000	10000
Experience collection epochs		500	1000	10000
Environment steps per epoch		200	500	100
Batch size ($\mathcal{V}, \mathcal{M}, \mathcal{C}$)		(128, 32, 128)	(-, 16, 128)	(-, 8, 128)
Training steps per epoch ($\mathcal{V}, \mathcal{M}, \mathcal{C}$)		(200, 200, 80)	(-, 300, 100)	(-, 100, 50)
Training start after epoch ($\mathcal{V}, \mathcal{M}, \mathcal{C}$)		(5, 25, 50)	(-, 15, 20)	(-, 250, 300)

Table 4: World model (\mathcal{M}) hyperparameters.

Description	Symbol	Atari-100K	DMC	Craftax
Number of layers		10	10	5
Number of heads		4	3	4
Embedding dimension	d	256	192	256
Dropout		0.1	0.1	0.1
Retention decay range	$[\eta_{\min}, \eta_{\max}]$	[4, 16]	[2, 2]	[8, 40]

Table 5: Actor-critic (\mathcal{C}) hyperparameters.

Description	Symbol	Atari-100K	DMC	Craftax
Environment reward weight	w^{ext}	1	1	100
Intrinsic reward weight	w^{int}	1	10	1
Encoder MLP (g_ψ) hidden layer sizes		[512]	[384]	[512, 512]
Shared backbone		True	False	True
Number of quantization values (continuous actions)			51	
(2D) Categoricals embedding dimension				64

Table 6: Atari 100K hyperparameters.

Description	Symbol	Value
Frame resolution		64×64
Frame Skip		4
Max no-ops (train, test)		(30, 1)
Max episode steps (train, test)		(20K, 108K)
Terminate on live loss (train, test)		(No, Yes)

Table 7: DeepMind Control Suite Proprioception hyperparameters.

Description	Symbol	Value
Action repeat		2

A.2. The Representation Module \mathcal{V}

A.2.1. IMAGE OBSERVATIONS

Image observations are tokenized using a vector-quantized variational auto-encoder (VQ-VAE) (van den Oord et al., 2017; Esser et al., 2021). A VQ-VAE comprises a convolutional neural network (CNN) encoder, an embedding table $\mathbf{E} \in \mathbb{R}^{n \times d}$, and a CNN decoder. Here, the size of the embedding table n determines the vocabulary size.

The encoder’s output $\mathbf{h} \in \mathbb{R}^{W \times H \times d}$ is a grid of $W \times H$ multi-channel vectors of dimension d that encode high-level learned features. Each such vector is mapped to a discrete token by finding the closest embedding in \mathbf{E} :

$$z = \arg \min_i \|\mathbf{h} - \mathbf{E}(i)\|$$

where $\mathbf{E}(i)$ is the i -th row of \mathbf{E} . To reconstruct the original image, the decoder first maps \mathbf{z} to their embeddings using \mathbf{E} . During training, the straight-through estimator (Bengio et al., 2013) is used for backpropagating the learning signal from the decoder to the encoder: $\hat{\mathbf{h}} = \mathbf{h} + \text{sg}(\mathbf{E}_z - \mathbf{h})$. The architecture of the encoder and decoder models is presented in Table 8.

The optimization objective is given by

$$\mathcal{L}(\text{enc}, \text{dec}, \mathbf{E}) = \|\mathbf{o} - \text{dec}(z)\|_2^2 + \|\text{sg}(\text{enc}(\mathbf{o}) - \mathbf{E}(z))\|_2^2 + \|\text{sg}(\mathbf{E}(z) - \text{enc}(\mathbf{o}))\|_2^2 + \mathcal{L}_{\text{perceptual}}(\mathbf{o}, \text{dec}(z))$$

where $\mathcal{L}_{\text{perceptual}}$ is a perceptual loss (Johnson et al., 2016; Larsen et al., 2016), proposed in (Micheli et al., 2023).

Crucially, the learned embedding table \mathbf{E} is used for embedding the (image) tokens across all stages of the algorithm.

A.2.2. CONTINUOUS VECTORS

The quantization of each feature uses 125 values (vocabulary size) in the range $[-6, 6]$, where 63 values are uniformly distributed in $[-\ln(1 + \pi), \ln(1 + \pi)]$ and the rest are uniformly distributed in the remaining intervals.

Table 8: The encoder and decoder architectures of the VQ-VAE model. “Conv(a,b,c)” represents a convolutional layer with kernel size $a \times a$, stride of b and padding c . A value of $c = \text{Asym.}$ represents an asymmetric padding where a padding of 1 is added only to the right and bottom ends of the image tensor. “GN” represents a GroupNorm operator with 8 groups, $\epsilon = 1e - 6$ and learnable per-channel affine parameters. SiLU is the Sigmoid Linear Unit activation (Hendrycks & Gimpel, 2017; Ramachandran et al., 2018). “Interpolate” uses PyTorch’s interpolate method with scale factor of 2 and the “nearest-exact” mode.

Module	Output Shape
Encoder	
Input	$3 \times 64 \times 64$
Conv(3, 1, 1)	$64 \times 64 \times 64$
EncoderBlock1	$128 \times 32 \times 32$
EncoderBlock2	$256 \times 16 \times 16$
EncoderBlock3	$512 \times 8 \times 8$
GN	$512 \times 8 \times 8$
SiLU	$512 \times 8 \times 8$
Conv(3, 1, 1)	$256 \times 8 \times 8$
EncoderBlock	
Input	$c \times h \times w$
GN	$c \times h \times w$
SiLU	$c \times h \times w$
Conv(3, 2, Asym.)	$2c \times \frac{h}{2} \times \frac{w}{2}$
Decoder	
Input	$256 \times 8 \times 8$
BatchNorm	$256 \times 8 \times 8$
Conv(3, 1, 1)	$256 \times 8 \times 8$
DecoderBlock1	$128 \times 16 \times 16$
DecoderBlock2	$64 \times 32 \times 32$
DecoderBlock3	$64 \times 64 \times 64$
GN	$64 \times 64 \times 64$
SiLU	$64 \times 64 \times 64$
Conv(3, 1, 1)	$3 \times 64 \times 64$
DecoderBlock	
Input	$c \times h \times w$
GN	$c \times h \times w$
SiLU	$c \times h \times w$
Interpolate	$c \times 2h \times 2w$
Conv(3, 1, 1)	$\frac{c}{2} \times 2h \times 2w$

A.3. The World Model \mathcal{M}

Embedding Details Each token in $\mathbf{z}^{(i)}$ of each modality is mapped to a d -dimensional embedding vector $\mathbf{X}^{(i)}$ using the embedding (look-up) table $\mathbf{E}^{(i)}$ of modality κ_i . The embedding vector that corresponds to token z is simply the z -th row in the embedding table. Formally, $\mathbf{x}_{t,j}^{(i)} = \mathbf{E}^{(i)}(l)$, $l = z_{t,j}^{(i)}$ where $\mathbf{E}(l)$ refers to the l -th row in \mathbf{E} . In the special case of 2D categorical inputs, $\mathbf{x}_{t,j}^{(i)} = \frac{1}{C} \sum_{n=1}^C \mathbf{E}_n^{(i)}(l_n)$, $l_n = z_{t,j,n}^{(i)}$ where C is the number of channels and i is the index of the 2D categorical modality in κ .

To concatenate the embeddings, we use the following order among the modalities: images, continuous vectors, categorical variables, and 2D categoricals.

Prediction Heads Each prediction head in \mathcal{M} is a multi-layer perceptron (MLP) with a single hidden layer of dimension $2d$ where d is the embedding dimension.

Epistemic Uncertainty Estimation Working with discrete distributions enables efficient entropy computation and ensures that the ensemble disagreement term δ_t is bounded by $\frac{1}{|\mathbf{z}_t|} \sum_{z \in \mathbf{z}_t} \log(\text{vocab_size}(z))$.

A.3.1. OPTIMIZATION

For each training example in the form of a trajectory segment in token representation $\tau = \mathbf{z}_1, \mathbf{a}_1, \dots, \mathbf{z}_H, \mathbf{a}_H$, the optimization objective is given by

$$\mathcal{L}_{\mathcal{M}}(\theta, \phi, \tau) = \sum_{t=1}^H \mathcal{L}_{\text{obs}}(\theta, \mathbf{z}_t, p_{\theta}(\hat{\mathbf{z}}_t | \mathbf{Y}_t^u)) + \mathcal{L}_{\text{reward}}(\theta, r_t, \hat{r}_t) - \log(p_{\theta}(d_t | \mathbf{Y}_t^u)) + \sum_{i=1}^{N_{\text{ens}}} \mathcal{L}_{\text{obs}}(\phi_i, \mathbf{z}_t, p_{\phi_i}(\hat{\mathbf{z}}_t | \text{sg}(\mathbf{Y}_t^u)))$$

where

$$\mathcal{L}_{\text{obs}}(\theta, \mathbf{z}_t, p_{\theta}(\hat{\mathbf{z}}_t | \mathbf{Y}_t^u)) = -\frac{1}{K} \sum_{i=1}^K \log p_{\theta}(z_i | \mathbf{y}_i)$$

is the average of the cross-entropy losses of the individual tokens, and $\mathcal{L}_{\text{reward}}(\theta, r_t, \hat{r}_t)$ is the $\mathcal{L}_{\text{HL-Gauss}}$ loss with the respective parameters of the reward head. Here, \mathbf{y}_i is the vector of \mathbf{Y}_t^u that corresponds to z_i , the i -th token of \mathbf{z}_t .

A.3.2. RETENTIVE NETWORKS

Retentive Networks (RetNet) (Sun et al., 2023) are sequence model architectures with a Transformer-like structure (Vaswani et al., 2017). However, RetNet replaces the self-attention mechanism with a linear-attention (Katharopoulos et al., 2020) based Retention mechanism. At a high level, given an input sequence $\mathbf{X} \in \mathbb{R}^{|\mathbf{X}| \times d}$ of d -dimensional vectors, the Retention operator outputs

$$\text{Retention}(\mathbf{X}) = (\mathbf{Q}\mathbf{K}^{\top} \odot \mathbf{D})\mathbf{V}$$

where $\mathbf{Q}, \mathbf{K}, \mathbf{V}$ are the queries, keys, and values, respectively, and \mathbf{D} is a causal mask and decay matrix. Notably, the softmax operation is discarded in Retention and other linear attention methods. As a linear attention method, the computation can also be carried in a recurrent form:

$$\begin{aligned} \text{Retention}(\mathbf{x}_t, \mathbf{S}_{t-1}) &= \mathbf{S}_t \mathbf{q}_t \\ \mathbf{S}_t &= \eta \mathbf{S}_{t-1} + \mathbf{v}_t \mathbf{k}_t^{\top} \in \mathbb{R}^{d \times d} \end{aligned}$$

where η is a decay factor, \mathbf{S}_t is a recurrent state, and $\mathbf{S}_0 = 0$. In addition, a hybrid form of recurrent and parallel forward computation known as the chunkwise mode allows to balance the quadratic cost of the parallel form and the sequential cost of the recurrent form by processing the input as a sequence of chunks. We refer the reader to (Sun et al., 2023) for the full details about this architecture.

In our implementation, since inputs are complete observation-action block sequences $\mathbf{X}_1, \dots, \mathbf{X}_t$, we configure the decay factors of the multi-scale retention operator in block units:

$$\eta = 1 - 2^{-\text{linspace}(\log(K\eta_{\min}), \log(K\eta_{\max}), N_h)}$$

where $\text{linspace}(a, b, c)$ is a sequence of c values evenly distributed between a and b , N_h is the number of retention heads, and η_{\min}, η_{\max} are hyperparameters that control the memory decay in observation-action block units.

A.3.3. PARALLEL OBSERVATION PREDICTION (POP)

POP (Cohen et al., 2024) is a mechanism for parallel generation of non-causal subsequences such as observations in token representation. It’s purpose is to improve generation efficiency by alleviating the sequential bottleneck caused by generating observations a single token at a time (as done in language models). However, to achieve this goal, POP also includes a mechanism for maintaining training efficiency. Specifically, POP extends the chunkwise forward mode of RetNet to maintain efficient training of the sequence model.

To generate multiple tokens into the future at once, POP introduces a set of prediction tokens $\mathbf{u} = u_1, \dots, u_K$ and embeddings $\mathbf{X}^u \in \mathbb{R}^{K \times d}$ where K is the number of tokens in an observation. Each token in \mathbf{u} corresponds to an observation token in \mathbf{z} . These tokens, and their respective learned embeddings, serve as a learned prior.

Let $\mathbf{X}_1, \dots, \mathbf{X}_T$ be a sequence of T observation-action (embeddings) blocks. Given \mathbf{S}_{t-1} summarizing all key-value outer products of elements of $\mathbf{X}_{\leq t-1}$, the outputs \mathbf{Y}^u from which the next observation tokens are predicted are given by:

$$(\cdot, \mathbf{Y}_t^u) = f_\theta(\mathbf{S}_{t-1}, \mathbf{X}^u)$$

Importantly, the recurrent state is never updated based on the prediction tokens \mathbf{u} (or their embeddings). The next observation tokens $\hat{\mathbf{z}}_t$ are sampled from $p_\theta(\hat{\mathbf{z}}_t | \mathbf{Y}_t^u)$. Then, the next action is generated by the controller, and the next observation-action block \mathbf{X}_t can be processed to predict the next observation $\hat{\mathbf{z}}_{t+1}$.

To maintain efficient training, a two step computation is carried at each RetNet layer. First, all recurrent states \mathbf{S}_t for all $1 \leq t \leq T$ are calculated in parallel. Although there is an auto-regressive relationship between time steps, the linear structure of \mathbf{S} allows to calculate the compute-intensive part of each state in parallel and incorporate past information efficiently afterwards. In the second step, all outputs \mathbf{Y}_t^u for all $1 \leq t \leq T$ are computed in parallel, using the appropriate states \mathbf{S}_{t-1} and \mathbf{X}^u in batch computation. Note that this computation involves delicate positional information handling. We refer the reader to (Cohen et al., 2024) for full details of this computation.

A.4. The Controller \mathcal{C}

Critic The value prediction uses 128 bins in the range $\mathbf{b} = (-15, \dots, 15)$.

Continuous Action Spaces The policy network outputs $m = 51$ logits corresponding to m quantization values uniformly distributed in $[-1, 1]$ for each individual action in the action vector.

A.4.1. INPUT ENCODING

The controller \mathcal{C} operates in the latent token space. Token trajectories $\tau = \mathbf{z}_1, \mathbf{z}_1^a, \dots, \mathbf{z}_H, \mathbf{z}_H^a$ are processed sequentially by the LSTM model. At each time step t , the network gets \mathbf{z}_t as input, outputs $\pi(\mathbf{a}_t | \tau_{\leq t-1}, \mathbf{z}_t)$ and $\hat{V}^\pi(\mathbf{a}_t | \tau_{\leq t-1}, \mathbf{z}_t)$, samples an action \mathbf{a}_t and then process the sampled action as another sequence element.

The processing of actions involve embedding the action into a latent vector which is then provided as input to the LSTM. Embedding of continuous action tokens is performed by first reconstructing the continuous action vector and then computing the embedding using a linear projection. Discrete tokens are embedded using a dedicated embedding table.

To embed observation tokens \mathbf{z} , the tokens of each modality are processed by a modality-specific encoder. The outputs of the encoders are concatenated and further processed by a MLP g_ψ that combines the information into a single vector latent representation.

The image encoder is a convolutional neural network (CNN). Its architecture is given in [Table 9](#).

Categorical variables are embedded using a learned embedding table. For 2D categoricals, shared per-channel embedding tables map tokens to embedding vectors, which are averaged to obtain a single embedding for each multi-channel token vector. For both types of categorical inputs we use 64 dimensional embeddings. The embeddings are concatenated and processed by g_ψ .

Table 9: The image observation encoder architecture of the actor-critic controller \mathcal{C} .

Module	Output Shape
Input	$256 \times 8 \times 8$
Conv(3, 1, 1)	$128 \times 8 \times 8$
SiLU	$128 \times 8 \times 8$
Conv(3, 1, 1)	$64 \times 8 \times 8$
SiLU	$64 \times 8 \times 8$
Flatten	4096
Linear	512
SiLU	512

A.4.2. OPTIMIZATION

λ -returns are computed for each generated trajectory segment $\hat{\tau} = (\mathbf{z}_1, \mathbf{a}_1, \bar{r}_1, d_1, \hat{\mathbf{z}}_2, \mathbf{a}_2, \bar{r}_2, d_2, \dots, \hat{\mathbf{z}}_H, \mathbf{a}_H, \bar{r}_H, d_H)$:

$$G_t = \begin{cases} \bar{r}_t + \gamma(1 - d_t)((1 - \lambda)\hat{V}_{t+1}^\pi + \lambda G_{t+1}) & t < H \\ \hat{V}_H^\pi & t = H \end{cases}$$

where $\hat{V}_t^\pi = \hat{V}^\pi(\hat{\tau}_{\leq t})$. These λ -returns are used as targets for critic learning. For policy learning, a REINFORCE ([Sutton et al., 1999](#)) objective is used, with a normalized \hat{V}^π baseline for variance reduction:

$$\mathcal{L}_\pi(\psi) = \mathbb{E}_\pi \left[\sum_{t=1}^H \text{sg} \left(\frac{G_t - \hat{V}_t^\pi}{\max(1, c)} \right) \log \pi(\mathbf{a}_t | \hat{\tau}_{\leq t-1}, \hat{\mathbf{z}}_t) + w_{\text{ent}} \mathcal{H}(\pi(\mathbf{a}_t | \hat{\tau}_{\leq t-1}, \hat{\mathbf{z}}_t)) \right]$$

where c is an estimate of the effective return scale similar to DreamerV3 ([Hafner et al., 2023](#)) and w_{ent} is a hyperparameter that controls the entropy regularization weight. c is calculated as the difference between the running average estimators of the 97.5 and 2.5 return percentiles, based on a window of return estimates obtained in the last 500 batches (imagination).

B. Implementation Details

Code We [open-source our code and trained model weights](#). Our code is written in Pytorch (Paszke et al., 2019). All code was developed by Lior Cohen. Experiments were run by Lior Cohen, Bingyi Kang, and Uri Gadot.

Hardware All Atari and DMC experiments were performed on V100 GPUs, while for Craftax a single RTX 4090 was used.

Run Times Experiments on Atari require approximately 12 hours on an RTX 4090 GPU and around 29 hours on a V100 GPU. For DMC, the runtime is about 40 hours on a V100 GPU. Craftax runs take roughly 94 hours, equivalent to 3.9 days.

Craftax The official environment provides the categorical variables in one-hot encoding format. Our implementation translates these variables to integer values which can be interpreted as tokens.

Setup in Atari Freeway For the Freeway environment, we adopted a modified sampling strategy where a temperature of 0.01 is used instead of the standard value of 1, following (Micheli et al., 2023; Cohen et al., 2024). This adjustment helps directing the agent toward rewarding paths. Note that alternative approaches in the literature tackle the exploration challenge through different mechanisms, including epsilon-greedy exploration schedules and deterministic action selection via argmax policies (Micheli et al., 2023).